

Proposal for a nanomechanical qubit

F. Pistolesi,¹ A.N. Cleland,² and A. Bachtold³

¹*Univ. Bordeaux, CNRS, LOMA, UMR 5798, F-33400 Talence, France*

²*Pritzker School of Molecular Engineering, University of Chicago, Chicago IL 60637, USA*

³*ICFO - Institut de Ciències Fotòniques, The Barcelona Institute of Science and Technology, 08860 Castelldefels, Barcelona, Spain*

(Dated: 25th of November 2020)

Mechanical oscillators have been demonstrated with very high quality factors over a wide range of frequencies. These also couple to a wide variety of fields and forces, making them ideal as sensors. The realization of a mechanically-based quantum bit could therefore provide an important new platform for quantum computation and sensing. Here we show that by coupling one of the flexural modes of a suspended carbon nanotube to the charge states of a double quantum dot defined in the nanotube, it is possible to induce sufficient anharmonicity in the mechanical oscillator so that the coupled system can be used as a mechanical quantum bit. This can however only be achieved when the device enters the ultrastrong coupling regime. We discuss the conditions for the anharmonicity to appear, and we show that the Hamiltonian can be mapped onto an anharmonic oscillator, allowing us to work out the energy level structure and how decoherence from the quantum dot and the mechanical oscillator are inherited by the qubit. Remarkably, the dephasing due to the quantum dot is expected to be reduced by several orders of magnitude in the coupled system. We also outline qubit control, readout protocols and how the qubit can be used as a static force quantum sensor.

I. INTRODUCTION

Mechanical systems have important applications in quantum information and quantum sensing, with for example significant recent interest in their use for frequency conversion between optical and microwave signals [1–6], the sensing of weak forces using position detection at or beyond the standard quantum limit [7], and demonstrations of mechanically-based quantum buses and memory elements [8–12]. Realizing a quantum bit (qubit) based on a mechanical oscillator is thus a highly desirable goal, providing the quantum information community with a new platform for quantum information processing and storage with a number of unique features. A hallmark of mechanical resonators is their ability to couple to a variety of external perturbations, as any force leads to a mechanical displacement; a mechanical qubit could thus enable quantum sensing [13] of a wide range of force-generating fields. Another outstanding aspect is that mechanical oscillators can be designed to exhibit very large quality factors [14, 15], thus well-isolated from their environment, with correspondingly long coherence times. Mechanical devices may offer the possibility to develop quantum circuits with both a large number of qubits and a long qubit decoherence time. This is of considerable relevance to quantum computing, since the decoherence times of superconducting qubits integrated in large scale circuits [16] are reduced to of order $10 \mu s$, which is much lower than what can be achieved when operating single superconducting qubits [17].

A mechanical oscillator can be made into a qubit by introducing a controlled anharmonicity, thereby introducing energy-dependent spacing in the oscillator's quantized energy spectrum [18, 19]. The anharmonicity then enables the controlled and selective excitation of energy states of the system, for example the ground and first

excited state, without populating other states, breaking the strong correspondence principle that otherwise limits the quantum control of harmonic systems.

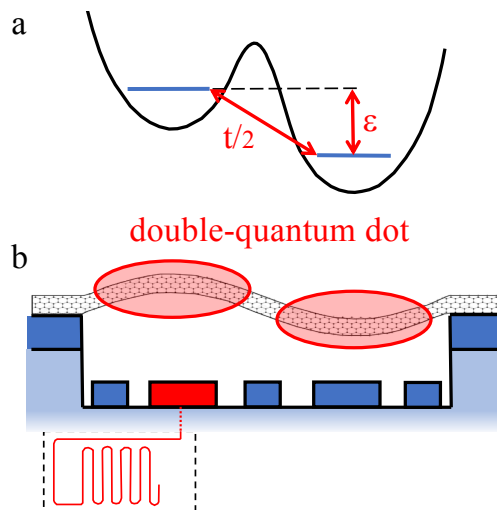


Figure 1. Schematic of the proposed setup. A suspended carbon nanotube hosting a double quantum dot, whose one-electron charged state is coupled to the second flexural mode. (a) Sketch of the electronic confinement potential and of the two main parameters, the hopping amplitude t and the energy difference ϵ between the two single-charge states. (b) Physical realization. One of the gate electrodes is connected to a microwave cavity for dispersive qubit readout.

Notwithstanding the apparent simplicity of this idea, finding mechanical oscillators with sufficiently strong and controllable anharmonicity is not trivial. In Ref. 18 and

19, anharmonicity induced by proximity to a buckling instability has been proposed. However, such a scheme is difficult to achieve experimentally. Here we consider the possibility of coupling one of the flexural modes of a carbon nanotube to an integrated double quantum dot, the dot itself defined in the nanotube, illustrated in Fig. 1. By tuning independently the gate voltages for the two quantum dots, it is possible to select the low-energy electronic states so that only those with a single (additional) electron on the double quantum dot are energetically accessible, where the excess electron can sit either on the left or the right dot. This charged two-level system is electrostatically coupled to the displacement of the oscillator, in particular to the second flexural mode, as illustrated in Fig. 1. We show in the following that for sufficiently strong electro-mechanical coupling, the double quantum dot induces a bistability in the mechanical mode, by reducing and then changing the sign of the quadratic term of the effective mechanical potential. We find that for strong but nonetheless reachable coupling constants, it is possible in this way to generate an anharmonicity sufficient to transform the mechanical oscillator into a qubit; this does however require entering the so-called ultrastrong coupling regime, where the coupling strength is larger than the mechanical energy level spacing. Remarkably, we also find that in the dispersive limit of large detuning of the oscillator frequency and the electronic two-level system energy splitting, the problem can be mapped onto the Hamiltonian of the quantum-anharmonic oscillator, allowing use of results from that system in this work. Following a description of the anharmonically-coupled system, we investigate the decoherence induced by the charged two-level system on the mechanical qubit, as well as how standard protocols for quantum manipulation can be implemented. The reduction of the pure-dephasing rate of the mechanical qubit with respect to that of the charged two-level system can be made larger than 10^3 with parameters accessible experimentally. We also show that the mechanical qubit can be used as a quantum sensor for any static force that could displace the oscillator. The static force sensitivity can reach values as good as $10^{-21}\text{N/Hz}^{1/2}$.

II. MODEL

We consider a nanomechanical system [20–27] based on a suspended carbon nanotube (cf. Fig. 1) similar to those demonstrated by a number of groups [28–31]. It has been shown that it is possible to use multiples gates to fine-tune the electrostatic potential along the suspended part of the nanotube [29, 32, 33]. It is thus possible to form a double-well potential to engineer a double quantum dot (cf. Fig. 1). We consider the case when only two states, each with one excess electron, are energetically accessible [34], the other states being at higher energy due to the Coulomb interaction. The two single-charge states, corresponding to an electron on the left or right dot, are

coupled by a hopping term $t/2$. Their relative energy difference, ϵ , can be controlled by varying the two gate voltages. The two states couple to the nanotube flexural modes. By placing the double dot in the center of the nanotube, the coupling of the two charge states with the second (anti-symmetric) mechanical mode is maximized [cf. Fig. 1]. A model Hamiltonian capturing the basic physics of this system can be written down:

$$H = \frac{p^2}{2m} + \frac{m\omega_m^2 x^2}{2} + \frac{\epsilon}{2}\sigma_z + \frac{t}{2}\sigma_x - \hbar g \frac{x}{x_z}\sigma_z, \quad (1)$$

where the first two terms describe the relevant mechanical mode of frequency $\omega_m/2\pi$ with effective mass m , displacement x , momentum p , and we have introduced the zero-point quantum fluctuation $x_z = (\hbar/2m\omega_m)^{1/2}$ with \hbar the reduced Planck constant. The electronic response has been reduced to a two-level system, where the two Pauli matrices σ_z and σ_x represent the dot charge energy splitting and inter-dot charge hopping, respectively. Finally $\hbar g/x_z$ is the variation of the force acting on the mechanical mode when the charge switches from one dot to the other. The value and sign of g can be tuned over a large range by adjusting the gate voltages [14].

In Appendix A we give a microscopic derivation of the Hamiltonian with the explicit form of the coupling terms.

III. BORN-OPPENHEIMER PICTURE

To gain an insight into the physics of the problem, it is instructive to first consider a semi-classical Born-Oppenheimer picture, valid for $\hbar\omega_m \ll \sqrt{t^2 + \epsilon^2}$. We diagonalize H given by Eq. (1), neglecting the p^2 term and regarding x as a classical variable. The two eigenvalues read:

$$\varepsilon_{\pm}(x) = m\omega_m^2 x^2/2 \pm \sqrt{(\epsilon - 2\hbar g x/x_z)^2 + t^2}/2. \quad (2)$$

In the spirit of Born-Oppenheimer approximation, the energy profile ε_{\pm} can be regarded as an effective potential for the oscillator, which depends on which charge quantum level is occupied. Taylor-expanding $\varepsilon_{\pm}(x)$ for small x and $\epsilon = 0$ one finds:

$$\varepsilon_{\pm} = \pm \frac{t}{2} + \frac{m\omega_m^2}{2} \left(1 \pm \frac{4\hbar g^2}{\omega_m t} \right) x^2 \mp \frac{4m^2\omega_m^2 \hbar^3 g^4}{t^3} x^4 + \dots \quad (3)$$

The coupling to the double dot leads to a renormalization of the quadratic coefficient and the appearance of a quartic (and higher) terms. The interaction stiffens the resonating frequency of the upper branch while softening the lower one. In particular, for $g > g_c^{\text{sc}} = (\omega_m t/4\hbar)^{1/2}$, the quadratic coefficient of the lower branch becomes negative. This leads to a double-well potential and a bistability similar to that predicted for a single quantum dot coupled to a mechanical oscillator [25, 27, 35–37].

Figure 2 shows the evolution of the two branches of the potential as a function of the coupling constant g , for

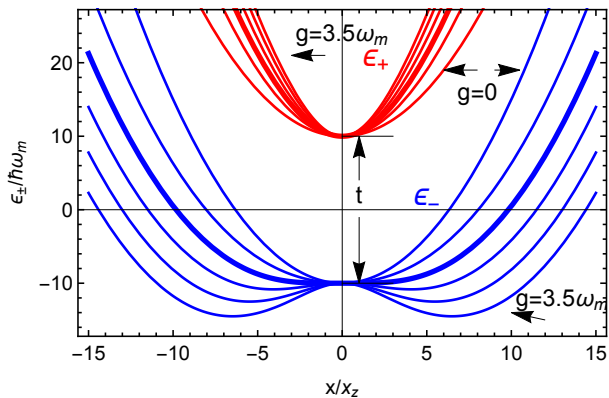


Figure 2. Effective potentials $\varepsilon_+(x)$ (red) and $\varepsilon_-(x)$ (blue) from Eq. (2) for $t/\hbar\omega_m = 20$ and the values of $(4g/\omega_m)^2 = 0, 10, 20, 30, 40, 50$, with the first and last line explicitly indicated in the figure. The potential for $g = g_c^{\text{sc}} = \omega_m\sqrt{5}$ is shown with a thicker line.

an experimentally-accessible value of $t = 20\hbar\omega_m$. One clearly sees the formation of the double well-potential for $g > g_c^{\text{sc}}$. For $g = g_c^{\text{sc}}$ the potential of the lower branch is purely quartic (thick line). Thus one expects that tuning g close to this critical value, it should be possible to modify, over a large range, the ratio between the quadratic and quartic terms and consequently tune the degree of anharmonicity of the system at will.

IV. FULL QUANTUM DESCRIPTION

A. Conditions for anharmonicity

The validity of the qualitative description of the previous section can be confirmed in the general case by numerical diagonalization of the Hamiltonian given by Eq. (1) in a truncated Hilbert space. Using a basis comprising the 10^2 lowest harmonic oscillator states largely suffices to reach convergence and we find the Hamiltonian eigenvectors $|n\rangle$ and eigenstates E_n for the problem. The result for the lowest set of energy levels is shown in Fig. 3.

We first notice that for $g \sim g_c^{\text{sc}}$, the ground state crosses the lowest non-interacting electronic level, indicated by the dashed line $-t/2$, preceding the formation of two bound states in the double-well. Note that one expects that this crossing should occur for a coupling larger than g_c^{sc} , since for this value the problem reduces to a quartic oscillator, for which the ground state has a positive value [38] similarly to the harmonic oscillator zero-point motion $\hbar\omega_m/2$. For $g \gg g_c^{\text{sc}}$, the two bound states have the same energy [cfr. the upper-right inset in Fig. 3] and are sufficiently far from each other that their overlap is negligible. In Fig. 3, the third level remains well separated from the first two, and merges with the

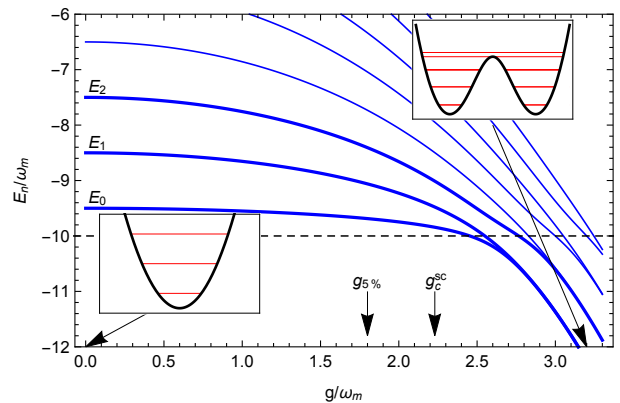


Figure 3. Lowest-lying energy eigenvalues E_n of the Hamiltonian (1) for $\epsilon = 0$ and $t = 20\hbar\omega_m$ as a function of g/ω_m . The Born-Oppenheimer potential given by Eq. (2) and the energy levels are shown in the insets for $g = 0$ and $g = 3.2\omega_m$. The dashed line indicates the lowest non-interacting electronic level $-t/2$. The semiclassical critical value for the bistability is $g_c^{\text{sc}}/\omega_m = \sqrt{5} \approx 2.23$. The value of $g = g_{5\%} \approx 1.8\omega_m$ for which the anharmonicity is 5% is also shown.

fourth level for large g . The anharmonicity, defined as

$$a = \frac{(E_2 - E_1) - (E_1 - E_0)}{E_1 - E_0}, \quad (4)$$

thus diverges as we increase g from 0 to a value of the order of g_c^{sc} . As discussed in the introduction, this anharmonicity is crucial to enabling quantum control of the qubit formed by the first two levels, $|0\rangle$ and $|1\rangle$. A minimum requirement is that the transition frequency between $|0\rangle$ and $|1\rangle$ needs to differ from that between $|1\rangle$ and $|2\rangle$ by much more than the spectral linewidth of the states. As a practical example, in the superconducting transmon qubit [39], an anharmonicity of the order of 5% suffices to afford full quantum control of the qubit states. In the following we will thus consider 5% anharmonicity as a (somewhat arbitrary) requirement; this is sufficient to find the relevant coupling scale required to implement the mechanical qubit.

Resorting again to numerical diagonalization, we present in Fig. 4 a contour plot for the dependence of the anharmonicity on the parameters t and g . The thick contour line for $a = 0.05$ defines the function $g_{5\%}$, which gives the required coupling to obtain a 5% anharmonicity. The region for $t < 2\hbar\omega_m$ presents a more complex structure. A weaker coupling is required to reach the needed anharmonicity. But in this region the first two levels inherit the properties of the double quantum dot to a large extent, so that we will not discuss it further. Here we explore the mechanical qubit in the parameter range when $t > 2\hbar\omega_m$, so that the nature of the two lowest energy states of the coupled system becomes mechanical. A sizable anharmonicity can only be reached when operating the device near or in the ultra-strong coupling regime, $g > \omega_m$, as seen in Fig. 4.

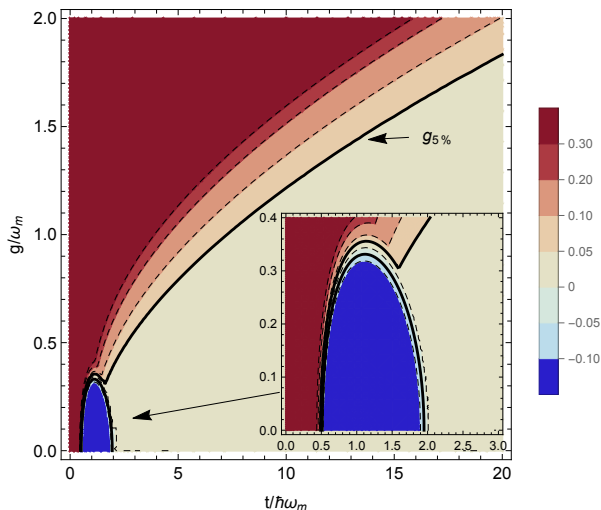


Figure 4. Contour plot of the anharmonicity a in the (t, g) plane. The contour line for $a = 0.05$ is thicker, and defines the function $g_{5\%}(t)$. The kink at $t \approx 1.54\hbar\omega_m$ of this function, better seen in the inset, is due to the avoided crossing between the charge and oscillator eigenstates that occurs at that value of t . It indicates the region where the eigenstate begins to have a predominantly charge nature.

B. Eigenstates

It is interesting to investigate the nature of the two qubit states $|0\rangle$ and $|1\rangle$. In the position representation, the wavefunction is given by $\psi_{n\sigma}(x) = \langle x, \sigma | n \rangle$, where $|n\rangle$ the Hamiltonian eigenstate and $|x, \sigma\rangle$ is the eigenstate of the displacement x and σ_z operators with eigenvalues x and σ , respectively. The wavefunction $\psi_{n\sigma}(x)$ can be chosen to be real-valued. Instead of looking directly at $\psi_{n\sigma}(x)$, it is more interesting to consider the averages of the operators σ_i as a function of x : $\langle \sigma_i \rangle(x) = \sum_{\sigma, \sigma'} \psi_{n\sigma}(x) [\sigma_i]_{\sigma\sigma'} \psi_{n\sigma'}(x)$. Since by symmetry $\langle \sigma_y \rangle = 0$, only $\langle \sigma_x \rangle = 2\psi_{n+}\psi_{n-}$ and $\langle \sigma_z \rangle = \psi_{n+}^2 - \psi_{n-}^2$ are non-vanishing.

We display in Fig. 5 these two components as well as the total probability for the oscillator displacement $\psi^2 = \psi_{n+}^2 + \psi_{n-}^2$ (blue curve in Fig. 5). The function $\langle \sigma_z \rangle(x)$ gives the distribution of the charge (green curve in Fig. 5), while $\langle \sigma_x \rangle(x)$ indicates the strength of the coherent superposition of the two charge-states (yellow curve in Fig. 5). These two quantities are in competition. From the figure, one sees that for weak coupling $\langle \sigma_z \rangle(x) \approx 0$, and the displacement probability distribution coincides with $-\langle \sigma_x \rangle(x)$. At the value of $g = g_{5\%}$, the distribution of the charge depends on x , for both states. Finally for the bistable case with $g/\omega_m = 3.0$, one reaches the limit where $|\langle \sigma_z \rangle(x)|$ is close to the displacement probability, indicating a full correlation between the displacement and the charge. We also show in the figure the distribution of the harmonic oscillator states. One clearly sees that for $g = g_{5\%}$, the two states are still

mainly eigenstates of the mechanical oscillator.

C. Mapping in the dispersive regime

The numerical diagonalization shows that the semiclassical picture provides a good qualitative description. A natural question is then how far one can extend this picture. For this reason, we looked for a unitary transformation U that could map the Hamiltonian given in Eq. (1) onto that of a simple anharmonic oscillator. In the limit of $g/|t/\hbar - \omega_m| \ll 1$, known as the dispersive limit, we find a U such that, at fourth order in g , we can write $H_T = U^\dagger H U$ with

$$H_T = \frac{t}{2}\sigma_z + \frac{\hbar\omega_m}{4} [\alpha_1\hat{p}^2 + \alpha_2\hat{x}^2 + \sigma_z(\alpha_3\hat{x}^2 + \alpha_4\hat{x}^4)]. \quad (5)$$

[We discarded the constant $\hbar^3 g^2 \omega_m / (t^2 - \hbar^2 \omega_m^2)$.] Here we introduce the quadratures $\hat{x} = x/x_z = a^\dagger + a$, $\hat{p} = p/(m\omega_m x_z) = i(a^\dagger - a)$, with $[\hat{x}, \hat{p}] = 2i$, where a and a^\dagger are the creation and destruction operators for the harmonic oscillator eigenstates. The four coefficients read

$$\alpha_1 = 1 + \frac{128\hbar^6 g^4 t^2 \omega_m^2}{\Delta^6 \Delta_3^2}, \quad \alpha_2 = 1 - \frac{16\hbar^4 g^4 t^2}{\Delta^4 \Delta_3^2}, \quad (6)$$

$$\alpha_3 = \frac{4\hbar t g^2}{\omega_m \Delta^2}, \quad \alpha_4 = -\frac{4\hbar^3 t g^4 (3t^2 + \hbar^2 \omega_m^2)}{3\omega_m \Delta^6}, \quad (7)$$

where $\Delta^2 = t^2 - (\hbar\omega_m)^2$, $\Delta_3^2 = t^2 - 9(\hbar\omega_m)^2$. The derivation and the definition of U are given in Appendix B.

Remarkably we find that within this approximation, it is possible to map the problem onto a new description with two anharmonic oscillators, one for each charge branch. The upper branch is unstable if we stop the expansion at x^4 , since it has a negative quartic term. This description thus holds for a small but non-zero value of the ratio $\hbar\omega_m/t$, giving a more accurate description than the simpler Born-Oppenheimer approach.

The anharmonic oscillator is a well-studied problem [40]. When the quadratic part is positive, it is convenient to write the lower branch of Eq. (5) in the standard form,

$$H = \hbar\omega'_m(\hat{x}^2 + \hat{p}^2 + \lambda\hat{x}^4)/4. \quad (8)$$

This can be done by the scaling $\hat{x} = \xi\hat{x}'$ and $\hat{p} = \hat{p}'/\xi$, so that the commutation relation is preserved $[\hat{x}', \hat{p}'] = 2i$, with

$$\xi = [\alpha_1/(\alpha_2 - \alpha_3)]^{1/4}, \quad (9)$$

The renormalized resonant frequency reads $\omega'_m = \omega_m[\alpha_1(\alpha_2 + \sigma\alpha_3)]^{1/2}$ and the quartic coefficient is

$$\lambda = \frac{\alpha_4\alpha_1^{1/2}}{(\alpha_2 - \alpha_3)^{3/2}}. \quad (10)$$

Note that we now consider only positive values of ω'_m , but Eq. (5) holds also in the bistable region. The anharmonicity a defined in Eq. (4) becomes a function of

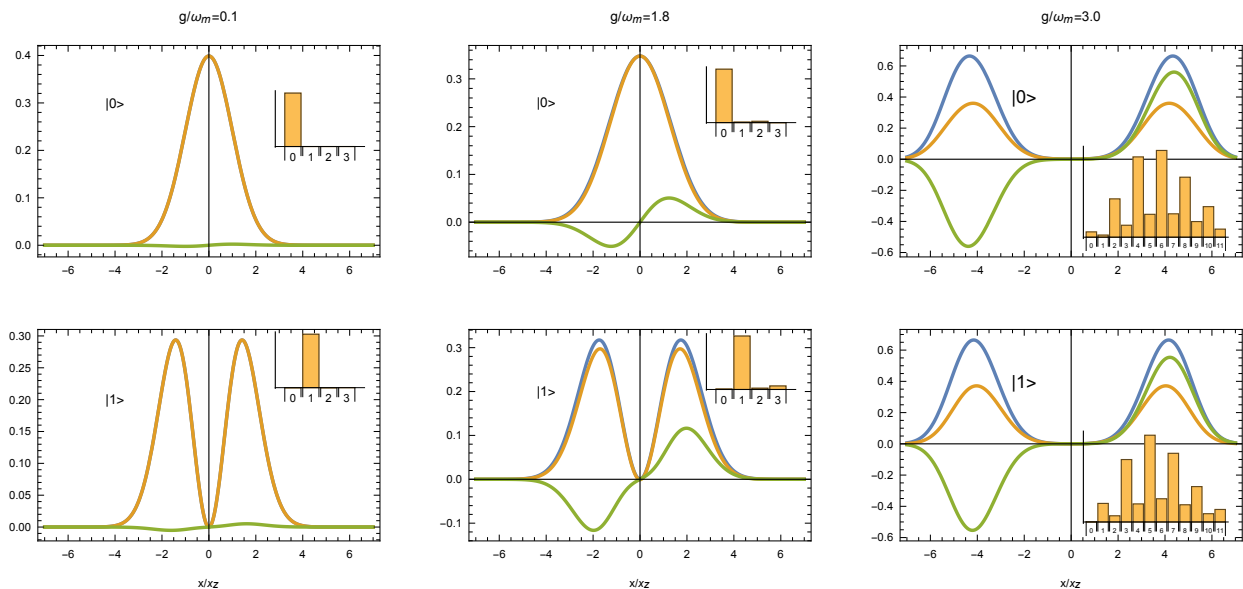


Figure 5. Wavefunctions of the two qubit states $|0\rangle$ (upper panels) and $|1\rangle$ (lower panels) for $t/\hbar\omega_m = 20$, $g/\omega_m = 0.1, 1.8$, and 3.0 . We plot $-\langle\sigma_x\rangle(x)$ (yellow), $\langle\sigma_z\rangle(x)$ (green), and $\psi_{n+}(x)^2 + \psi_{n-}(x)^2$ (blue). Note that for small coupling the yellow and blue lines perfectly overlap. The probability of occupation of the first single-harmonic oscillator states are indicated in the insets.

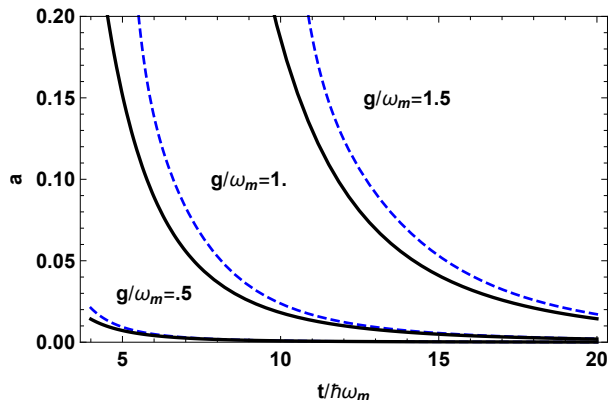


Figure 6. Comparison between numerical (full line) and analytical (dashed line) dependence of the anharmonicity parameter a for three values of the coupling $g/\omega_m = 0.5, 1, 1.5$.

λ only. Using the expression (1.17) of Ref. 40 for the eigenvalues in terms of λ and Eq. (10), one can obtain an analytical expression for the anharmonicity in terms of the parameters ω_m , t , and g with a reasonable accuracy, as can be seen in Fig. 6. One finds that the 5% anharmonicity is achieved for $\lambda_c \approx 0.0225$ (the exact numerical result is $\lambda_c = 0.0220$).

D. Operators acting on the qubit

In order to study the control, readout, and decoherence of the qubit formed by the two states $|0\rangle$ and $|1\rangle$, it is necessary to find the projection of the physical operators

σ_i , \hat{x} , and \hat{p} in the Hilbert space spanned by these states $\{|0\rangle, |1\rangle\}$. In this space, any operator can be written as a linear combination of the unit matrix (τ_0) and the three Pauli matrices, that we define here as $\{\tau_x, \tau_y, \tau_z\}$, to distinguish them from the operators σ_i acting in the charge space. The Hamiltonian of the qubit then simply reads $(E_1 - E_0)\tau_z/2$. One can calculate numerically the matrix elements of any operator in the qubit sub-space and then obtain its form in terms of a sum of the four τ -matrices. We find for the charge variables

$$\begin{cases} \sigma_x|_{\text{qb}} = \beta_1\tau_0 + \beta_2\tau_z, \\ \sigma_y|_{\text{qb}} = \beta_3\tau_y, \\ \sigma_z|_{\text{qb}} = \beta_4\tau_x, \end{cases} \quad (11)$$

and for the oscillator variables

$$\begin{cases} \hat{x}|_{\text{qb}} = \beta_5\tau_x, \\ \hat{p}|_{\text{qb}} = \beta_6\tau_y. \end{cases} \quad (12)$$

The six coefficients can be obtained numerically, but it is also interesting to obtain approximate analytical expressions for them. This can be achieved using the unitary

transformation introduced above (see Appendix B):

$$\beta_1 = -1 + 4(\hbar g)^2 \frac{(\hbar\omega_m)^2 - t\hbar\omega_m\xi^2 + t^2\xi^4}{\Delta^4\xi^2} + g^4\beta_{1,4}, \quad (13)$$

$$\beta_2 = -2(\hbar g)^2 \frac{(\hbar\omega_m)^2 + t^2\xi^4}{\Delta^4\xi^2} + g^4\beta_{2,4}, \quad (14)$$

$$\beta_3 = \frac{2\hbar^2 g\omega_m}{\Delta^2\xi} + g^3\beta_{3,3}, \quad (15)$$

$$\beta_4 = \frac{2\hbar g t \xi}{\Delta^2} + g^3\beta_{4,3}, \quad (16)$$

$$\beta_5 = \xi - \frac{2\hbar^3 g^2 t \omega_m \xi}{\Delta^4} + g^4\beta_{5,4}, \quad (17)$$

$$\beta_6 = \frac{1}{\xi} - \frac{2\hbar^3 g^2 t \omega_m}{\Delta^2\xi} + g^4\beta_{6,4}. \quad (18)$$

The coefficients for g^3 and g^4 are given by Eqs. (B16)-(B21) in the Appendix.

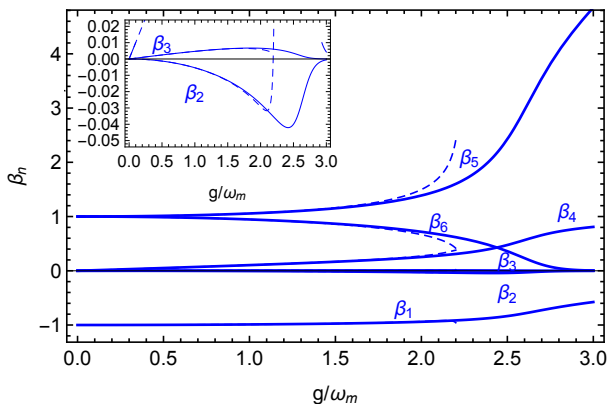


Figure 7. Coefficients β_i of the operator projections in the qubit space, obtained by numerical diagonalization (full lines) and from the analytical approximation to fourth order in g (dashed lines). The value of t is fixed here to $20\hbar\omega_m$.

We show in Fig. 7 the behavior of the analytic coefficients as a function of g/ω_m for $t/\hbar\omega_m = 20$, and compare to the exact numerical results. The analytical expressions again give a good description in the interesting range $g < g_{5\%}$. In particular, these expressions allow us to recognize that β_2 and β_3 are parametrically small for $g \approx \omega_m \ll t/\hbar$.

Another important result given by the expressions for the β_i is the charge component of the qubit. This can be identified with the value of the β_4 coefficient, which gives the projection of the charge operator σ_z in the qubit space. This coefficient vanishes linearly in g , and it remains small up to $g \approx \sqrt{\omega_m t/\hbar}$ when $t \gg \hbar\omega_m$. In this case, we thus expect that the qubit has a predominantly mechanical character in its degrees of freedom, measured by the β_5 and β_6 coefficients, which remain of the order of unity.

E. Qubit Manipulation

The values of β are also crucial to understanding how to manipulate the qubit. This is achieved using a completely classical oscillating voltage applied to a nearby wire, turned on for some duration with a calibrated amplitude. The anharmonicity of the system allows this classical signal to achieve quantum control. One can find the effect of an oscillating voltage on the qubit by considering how this voltage couples to the σ_i and \hat{x} operators. In Appendix A, we derive these couplings for a potential V_{g12}^{AC} coupled asymmetrically to the two gates controlling the electrochemical potential of each dot [cfr. Eq. (A23)]. We find that the potential couples to σ_z and \hat{x} with the coefficients λ^{ev}/e and $\lambda^{\text{mv}}x_z$, respectively (see Appendix A for the explicit expressions). Since both \hat{x} and σ_z project on τ_x , we find that the coupling to the oscillating field is just $\lambda_v \tau_x V_{g12}^{\text{AC}}$ with

$$\lambda_v = \lambda^{\text{mv}}x_z\beta_5 + \lambda^{\text{ev}}\beta_4/e. \quad (19)$$

This indicates that one can use standard methods to manipulate the qubit state, *e.g.* by using nuclear magnetic resonance methods by driving the qubit states at a frequency ω_D with pulses that induce, in the rotating frame, a term $(E_1 - E_0 - \hbar\omega_D)\tau_z/2 + \lambda_v V_{g12}^0 \tau_x$ [41]. The anharmonicity guarantees that the second excited state will not be populated by these manipulations.

F. Qubit Readout

Reading out the state of the qubit can be realised by coupling the system to a microwave superconducting cavity and using a dispersive interaction, analogous to what is done with superconducting qubits [42, 43]. The coupling can be obtained from the expression of the coupling to an oscillating voltage (cfr. A21 and A22) with the substitution $V^{\text{AC}} \rightarrow V_z(b + b^\dagger)$, where b is the destruction operator of the photons in the cavity and V_z is the zero-point motion voltage of the cavity. The coupling Hamiltonian reads

$$H^{\text{qb-cav}} = \hbar g_v \tau_x (b + b^\dagger) \quad (20)$$

with $g_v = \lambda_v V_z$ (cfr. Eq. (19)). A standard method is then to perform a dispersive measurement of the superconducting cavity frequency, which is modified by a slightly different amount depending on the qubit state. By performing a standard unitary transformation [44] one can eliminate the τ_x term and obtain for the qubit and cavity Hamiltonian

$$H = (E_1 - E_0)\tau_z/2 + (\hbar\omega_c + \chi\tau_z)b^\dagger b \quad (21)$$

where ω_c is the cavity resonating frequency and $\chi = \hbar^2 g_v^2 / (E_1 - E_0 - \hbar\omega_c)$ the dispersive shift. Since the resonating frequency depends now on the qubit state, this allows us to perform an efficient quantum non-destructive readout of the qubit state.

The proposed system allows also another possibility. Detection of the qubit can be realised by coupling the system to a microwave cavity tuned at the transition frequency $(E_{n_0} - E_0)/\hbar$ between the ground state and the high-energy state n_0 . The occupation of the ground state can be detected by measuring the photon transmitted phase [45]. Since the microwave cavity couples mainly to the charge, the ideal high-energy state should have a large matrix element with the σ_z operator: $\langle n_0 | \sigma_z | 0 \rangle$. The main difficulty of this approach is that the excited state $|1\rangle$ could also have a large overlap with the same operator to an other state, say n_1 . In order to be able to discriminate these two cases one needs that the anharmonicity for these states, $a' = [(E_{n_1} - E_1) - (E_{n_0} - E_0)] / (E_{n_0} - E_0)$, is sufficiently large. We choose for n_0 and n_1 the two states that maximize the matrix element of σ_z with the ground and the first excited states, respectively. For weak coupling n_0 (n_1) is given by the mechanical oscillator in the ground (first excited) state and the double dot in the excited state. We plot in Fig. 8 the ratio a' for $g = g_{5\%}$ as a function of $t/\hbar\omega_m$.

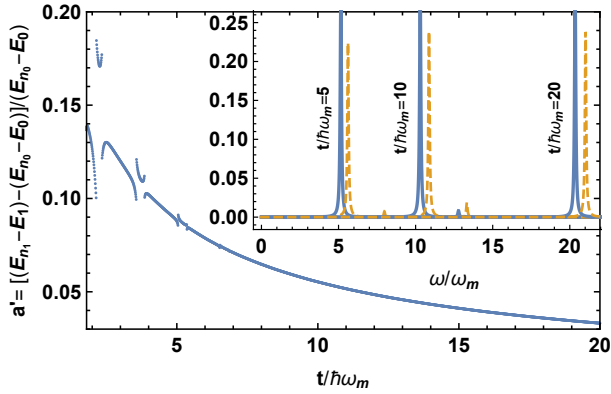


Figure 8. Anharmonicity for the higher excited states: $a' = [(E_{n_1} - E_1) - (E_{n_0} - E_0)] / (E_{n_0} - E_0)$ as a function of $t/\hbar\omega_m$ for $g = g_{5\%}$. The anharmonicity is sufficient to allow a detection of the qubit state by spectroscopy. Inset: expected spectrum (with a $0.1\omega_m$ added width) obtained with a signal coupling to σ_z for three different values of $t/\hbar\omega_m$ and $g = g_{5\%}(t)$. The full (dashed) line is the signal for the transition $|0\rangle \rightarrow |n\rangle$ ($|1\rangle \rightarrow |n\rangle$). The main peak are obtained for the case $n = n_0$ ($n = n_1$).

We find that for $t < 20\omega_m$, the anharmonicity a' remains larger than 4%, thus being of the same order or larger than the anharmonicity a of the first two excited qubit states. This proves that one can therefore also use this state spectroscopy method to read out the qubit state.

V. DECOHERENCE

The double quantum dot and the mechanical oscillator are unavoidably coupled to the environment, which

induces decoherence and incoherent transitions between energy levels. The decoherence rate of the double quantum dot charge qubit is much larger than that of the mechanical resonator, so that it will limit the performances of the mechanical qubit. Best values for the decoherence rate are in the MHz range [46].

In order to study how the nano-mechanical qubit inherits the decoherence of its two sub-system components, we begin by constructing a simple model for the coupling of the sub-systems to the environment.

We write the coupling Hamiltonian as

$$H_I = \hat{A}^c \hat{E}_1 + \hat{x} \hat{E}_2, \quad (22)$$

where $\hat{A}^c = \sum_{i=x,y,z} v_i \sigma_i = \vec{v} \cdot \vec{\sigma}$ is the most general operator in the charge subspace (see for instance [47]). The operators \hat{E}_1 and \hat{E}_2 are given by the sum of operators, themselves involving many degrees of freedom that model the environment of the charge and the mechanical oscillator, respectively (the coupling constant is absorbed in the \hat{E} -operators so that \hat{A}^c and \hat{x} are dimensionless). We assume that we know the correlation functions $C_i(t) = \langle \hat{E}_i(t) \hat{E}_i(0) \rangle$, as well as their Fourier transforms $S_i(\omega) = \int dt e^{i\omega t} C_i(t)$, and that the charge and mechanical environments are independent, $\langle \hat{E}_1(t) \hat{E}_2(0) \rangle = 0$. If $S_i(\omega)$ is a sufficiently smooth function for ω close to the qubit resonant frequency, the three parameters v_i give a complete description of the coupling to the environment of the charge system. For the mechanical oscillator, we parametrize the coupling to the environment with a single damping rate γ .

One can then use the standard procedure, integrating out the environmental degrees of freedom and finding an equation for the reduced density matrix ρ in the Born-Markov and rotating-wave approximations. The rate equations have the standard form:

$$\dot{\rho}_{nn} = -\rho_{nn} \sum_{p \neq n} \Gamma_{n \rightarrow p} + \sum_{p \neq n} \rho_{pp} \Gamma_{p \rightarrow n}, \quad (23)$$

$$\dot{\rho}_{nm} = - \left[\sum_{p \neq n} \Gamma_{n \rightarrow p} / 2 + \sum_{p \neq m} \Gamma_{m \rightarrow p} / 2 + \Gamma_{nm}^\phi \right] \rho_{nm}, \quad (24)$$

where $\rho_{nm} = \langle n | \rho | m \rangle$ is the matrix element of ρ in the eigenstate basis $|n\rangle$ of the Hamiltonian (1) with eigenvalues E_n . The rates read:

$$\Gamma_{n \rightarrow m} = 2\pi S_1(\omega_{nm}) |A_{nm}^c|^2 + 2\pi S_2(\omega_{nm}) |x_{nm}|^2, \\ \Gamma_{nm}^\phi = \pi S_1(0) (A_{nn}^c - A_{mm}^c)^2 + \pi S_2(0) (x_{nn} - x_{mm})^2$$

where $\omega_{nm} = (E_n - E_m)/\hbar$, $O_{nm} = \langle n | O | m \rangle$, and Γ_{nm}^ϕ is the pure dephasing rate. These equations hold at non-zero temperature T , with $S_i(\omega) = S_i(-\omega) e^{\hbar\omega/k_B T}$ and k_B is the Boltzmann constant. When only two levels are present one finds

$$\dot{\rho}_{00} = -\rho_{00} \Gamma_{0 \rightarrow 1} + \rho_{11} \Gamma_{1 \rightarrow 0} \quad (25)$$

$$\dot{\rho}_{01} = -\rho_{01} (\Gamma_{0 \rightarrow 1} + \Gamma_{1 \rightarrow 0} + 2\Gamma_{01}^\phi) / 2. \quad (26)$$

The last equation defines the coherence time of the qubit $T_2 = 2/(\Gamma_{0 \rightarrow 1} + \Gamma_{1 \rightarrow 0} + 2\Gamma_{01}^\phi)$. In the following we focus on the two rates $\Gamma_{1 \rightarrow 0}$ and Γ_{01}^ϕ . (We do not consider the case of equally-spaced levels inducing transfer of coherence between higher energy states [48].)

A. Non-interacting case

Let us begin with the non-interacting case ($g = 0$) in order to define the rates. We have two independent systems: the double quantum dot and the mechanical oscillator. For the oscillator, one finds $\Gamma_{1 \rightarrow 0}^m = 2\pi S_2(\omega_m) = \gamma(1 + n_{\text{th}})$, where $n_{\text{th}} = 1/(e^{\hbar\omega_m/k_B T} - 1)$ and $\Gamma_{12}^{m,\phi} = 0$. For the charge system, we begin by diagonalizing the Hamiltonian $H_0 = (\epsilon\sigma_z + t\sigma_x)/2$, performing a rotation by an angle $\theta = \arctan(t/\epsilon)$ around the y axis: $U(\theta) = e^{-i\theta\sigma_y/2}$. One has

$$U(\theta)^\dagger \sigma_x U(\theta) = \cos\theta\sigma_x - \sin\theta\sigma_z, \quad (27)$$

$$U(\theta)^\dagger \sigma_z U(\theta) = \sin\theta\sigma_x + \cos\theta\sigma_z, \quad (28)$$

with σ_y invariant. The charge Hamiltonian coupled to the environment then becomes

$$H' = U^\dagger H U = \frac{1}{2}\sqrt{t^2 + \epsilon^2}\sigma_z + \vec{v}'\vec{\sigma}\hat{E}_1, \quad (29)$$

with $v'_x = \cos\theta v_x + \sin\theta v_z$, $v'_z = -\sin\theta v_x + \cos\theta v_z$, and $v'_y = v_y$. This gives the rates

$$\Gamma_{1 \rightarrow 0}^c(\theta) = 2\pi S_1\left(\sqrt{\epsilon^2 + t^2}\right) [(\cos\theta v_x + \sin\theta v_z)^2 + v_y^2], \quad (30)$$

$$\Gamma_{01}^{c,\phi}(\theta) = 4\pi S_1(0)(\sin\theta v_x - \cos\theta v_z)^2. \quad (31)$$

According to these equations, the pure dephasing and decay rates depend on the value of θ (i.e. the ratio ϵ/t). Since the environmental spectrum depends only on the charge energy splitting, the ratios

$$R^D \equiv \frac{\Gamma_{0 \rightarrow 1}^c(0)}{\Gamma_{0 \rightarrow 1}^c(\pi/2)} = \frac{v_x^2 + v_y^2}{v_z^2 + v_x^2}, \quad (32)$$

$$R^\phi \equiv \frac{\Gamma_{01}^{c,\phi}(0)}{\Gamma_{01}^{c,\phi}(\pi/2)} = \frac{v_z^2}{v_x^2}, \quad (33)$$

depend only on the values of v_i . One can then, at least in principle, measure the rates for the same energy splitting $\sqrt{t^2 + \epsilon^2}$ and the two values of θ , 0 and $\pi/2$. This gives R^D and R^ϕ that can be used to express v_y and v_z in terms of v_x :

$$v_y^2 = [R^D(1 + R^\phi) - 1]v_x^2, \quad (34)$$

$$v_z^2 = R^\phi v_x^2. \quad (35)$$

B. Interacting case

We can now consider the interacting case. We will exploit the fact that the operators σ_i and \hat{x} in the subspace

spanned by $\{|0\rangle, |1\rangle\}$ can be written in terms of the τ_i operators [Eq. (11) and Eq. (12)]. We neglect the decay rate from and to the third level, which is small as it is only due to oscillator damping and vanishes exponentially for $k_B T \ll \hbar\omega_m$. We obtain then the following results for the decay and decoherence rate of the nanomechanical qubit:

$$\Gamma_{1 \rightarrow 0}^{\text{qb}} = 2\pi S_1(\omega_{10})(v_z^2\beta_4^2 + v_y^2\beta_3^2) + 2\pi S_2(\omega_{10})\beta_5^2,$$

$$\Gamma_{01}^{\text{qb},\phi} = 4\pi S_1(0)v_x^2\beta_2^2.$$

Using the relations (34)-(35) and assuming that $S_i(\omega_{10}) \approx S_i(\omega_m)$, we find

$$\Gamma_{1 \rightarrow 0}^{\text{qb}} = \Gamma_{1 \rightarrow 0}^c(\pi/2) \frac{R_\phi\beta_4^2 + [R^D(1 + R^\phi) - 1]\beta_2^2}{1 + R^\phi} + \beta_5^2\gamma(1 + n_{\text{th}}) \quad (36)$$

$$\Gamma_{01}^{\text{qb},\phi} = \beta_2^2\Gamma_{01}^{c,\phi}(\pi/2). \quad (37)$$

In the region of interest, we can use the analytical expressions for β_i . For $\hbar\omega_m/t \ll 1$ we can drop the term proportional to $\beta_2^2 \ll \beta_4^2$ and obtain

$$\Gamma_{1 \rightarrow 0}^{\text{qb}} \approx \frac{R_\phi}{1 + R^\phi} \frac{4\hbar^2 g^2 t^2 \omega_m}{\Delta^4 \omega'_m} \Gamma_{1 \rightarrow 0}^c(\pi/2) + \frac{\omega_m}{\omega'_m} \left[1 - \frac{4\hbar^3 g^2 t \omega_m}{\Delta^4} \right] \gamma(1 + n_{\text{th}}). \quad (38)$$

The pure dephasing is controlled by $\beta_2^2 \approx (\hbar g/t)^4 \ll 1$. The dephasing is thus strongly reduced in the nanomechanical qubit in comparison to the charge system.

We can evaluate numerically the reduction of the decay and pure-dephasing rates for the case $R^D = R^\phi = 1$. The result for $\Gamma_{1 \rightarrow 0}^{\text{qb}}(g_{5\%})/\Gamma_{1 \rightarrow 0}^{\text{qb}}(g = 0)$ and $\Gamma_{10}^{\text{qb},\phi}(g_{5\%})/\Gamma_{10}^{\text{qb},\phi}(g = 0)$ is shown in Fig. 9 as a function of t for $\gamma = 0$. As expected from the analytical expressions, the larger the value of t , the larger the reduction in the decoherence. This is a natural consequence of the mechanical nature of the qubit in this limit.

VI. PROSPECT FOR EXPERIMENTAL IMPLEMENTATION

The results found in the two previous sections are very promising for the experimental realization of a nanomechanical qubit. In this section we discuss possible experimental implementations using currently available technology. As discussed in the introduction, the double quantum dot can be realized in a suspended carbon nanotube and coupled to the second mechanical flexural mode of the nanotube. Such a device has been recently measured at 2 K [29], reporting values $t/2\pi\hbar = 49 - 96$ GHz with a tunable value of ϵ , a second mechanical mode of frequency $\omega_m/2\pi = 327$ MHz with a mechanical quality factor $Q = 4 \cdot 10^3$ and a coupling constant $g/2\pi = 320$ MHz. Taking these parameters, we have $t/\hbar\omega_m$ up to 150-300, and $g/\omega_m \approx 1$, noting that of course t can be

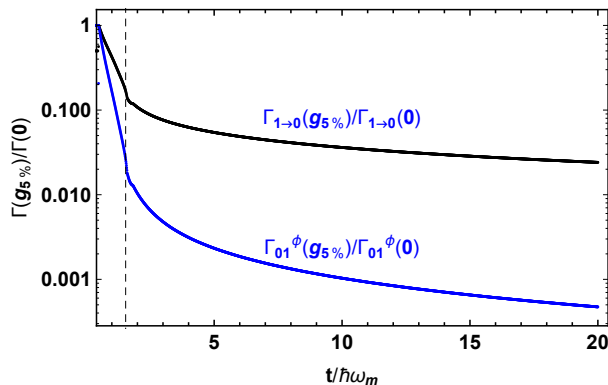


Figure 9. Ratio of the decay rate $\Gamma_{1 \rightarrow 0}^{\text{qb}}(g_{5\%})/\Gamma_{1 \rightarrow 0}^{\text{qb}}(g=0)$ and pure decoherence rate $\Gamma_{10}^{\text{qb},\phi}(g_{5\%})/\Gamma_{10}^{\text{qb},\phi}(g=0)$ as a function of $t/\hbar\omega_m$. We assume $R^D = R^\phi = 1$ and we neglect oscillator damping ($\gamma = 0$). The vertical dashed line indicates the beginning of the region where the qubit becomes dominated by the two charge states, i.e. where $t < 1.54\hbar\omega_m$ (cfr. also inset of Fig. 4).

tuned to lower values. Choosing $t = 7\hbar\omega_m$, we can operate on the $g_{5\%}$ line (cfr. Fig. 4) without changing other parameters. At this value of g , we already have a sizeable reduction of both the decoherence and decay rates of the mechanical qubit $\Gamma_{1 \rightarrow 0}$ and Γ_{10}^ϕ [cfr. Fig. 9] compared to that of the charge double quantum dot. The experiment at 2 K realized with a device fabricated on a Si substrate reports an incoherent tunnelling rate $\Gamma_{1 \rightarrow 0}$ estimated to $2\pi \cdot 510$ MHz, which is clearly too large to use for qubit operations, but improvements should be possible, by operating the device at 10 mK to suppress the decoherence induced by low-frequency vibrations (phonon) modes, by producing devices on sapphire substrates that host a minimal number of charge fluctuators, and by current-annealing the nanotube in-situ in the dilution fridge to remove all the contamination adsorbed on the surface of the nanotube [49]. Double-dot structures have been created in non-suspended carbon nanotubes, and have been coupled to superconducting cavities [50].

One can thus target a mechanical resonator cooled at 10 mK with $\omega_m/2\pi$ in the range of 0.6-1 GHz using a nanotube that is shorter and/or is under mechanical tension. A value of $t/\hbar\omega_m = 10$ will then require a coupling constant of the order of $1.1\hbar\omega_m$, which can be obtained by reducing the nanotube-gate separation and/or increasing the voltage applied on the gate electrode. With these values the reduction of the pure-dephasing decoherence rate of the mechanical qubit with respect to that of the double quantum dot will be about 10^3 . Assuming that the decoherence rate of the order of 3 MHz can be obtained, as was achieved in GaAs coupled double quantum dots [46] and that it is mainly limited by pure dephasing, it should be possible to implement most of the standard protocols for quantum computation using a mechanical

qubit with a 3 kHz decoherence rate.

Another possible implementation consists in using a nonsuspended GaAs double quantum dot with 3 MHz charge decoherence rate coupled to a suspended metal beam, such as a carbon nanotube.

VII. QUANTUM SENSING OF A STATIC FORCE WITH THE NANOMECHANICAL QUBIT

As an interesting application, we discuss here the possibility of using the nanomechanical qubit for quantum sensing. A mechanical oscillator can couple to a variety of forces; independently of the nature of the force, the additional term in the Hamiltonian describing this coupling can be written as $H_F = Fx$, with F the external force. In terms of the nanomechanical qubit operators this gives $H_F = F\gamma_F\tau_x/2$, with $\gamma_F = 2x_z\beta_5$ (cf. Eq. (12) and we introduced a factor of two for convenience in the notation). One can then use the protocols for qubit preparation and read-out in order to measure F with great sensitivity.

As a relevant example we consider here the Rabi measurement protocol, as described in Ref. [13] sec. IV.D. In a nutshell it consists in preparing the qubit in the ground state, and then let it evolve in the presence of the static force F according to the Hamiltonian

$$H = \hbar(\omega_0\tau_z + \omega_1\tau_x)/2, \quad (39)$$

with angular frequencies $\omega_0 = (E_2 - E_1)/\hbar$ and $\omega_1 = F\gamma_F/\hbar$. This induces a Larmor-like precession with a Rabi frequency $\omega_R = \sqrt{\omega_0^2 + \omega_1^2}$ of the pseudo spin representing the qubit state in the Bloch sphere around the direction of the effective magnetic field vector $(\omega_1, 0, \omega_0)$. The probability P_1 of measuring the qubit in the excited state oscillates as

$$P_1 = \frac{\omega_1^2}{\omega_R^2} \sin^2(\omega_R t/2). \quad (40)$$

For large t the sine part of the expression is very sensitive to a small variation of ω_R and thus of the force. For a detection time t_d such that $\omega_R t_d = \pi/2 + k\pi$, with k a large integer one finds

$$\delta P_1 \approx \left(\frac{\omega_1}{\omega_R}\right)^3 \frac{\gamma_F t_d}{2\hbar} F. \quad (41)$$

The sensitivity thus increases with the oscillation time t_d . This is mainly limited by the coherence time of the qubit. One also sees that in order to have a large signal it is better to have ω_1 of the same order or larger than ω_0 . In our case this could be achieved using the gate voltage that generates an additional controllable static force to the oscillator. The most fundamental source of uncertainty in quantum sensing is the binomial fluctuation of the qubit readout outcome. Following Ref. [13] a rough estimate of the signal to noise that can be achieved with this method

gives that the minimum detectable static force with a 1 second measurement is

$$\delta F_{\min} \approx \frac{\hbar}{\gamma_F \sqrt{T_2}}, \quad (42)$$

where T_2 is the coherence time.

Using typical values for carbon nanotube resonators $\omega_m = 2\pi \cdot 500$ MHz, $m = 10^{-21}$ Kg, one has $x_z = 4 \cdot 10^{-12}$ m. Using $T_2 \sim 50\mu\text{s}$ from the 3 kHz decoherence rate for the nanotube mechanical qubit estimated in the last section, the static force sensitivity is $\sim 10^{-21}$ N/Hz^{1/2}. For comparison, the resolution in static force measurements is 10^{-17} N using optically levitated particles [51] and 10^{-12} N with atomic force cantilevers in high vacuum and at low temperatures [52], while a sensitivity of 10^{-15} N/Hz^{1/2} can be achieved using optical tweezers in liquids [53]. One finds that when the electronic contribution to the decoherence can be neglected with respect to the mechanical part, then quantum sensing can reach sensitivities of the order of the standard quantum limit [54].

VIII. CONCLUSIONS

In conclusion we have shown that coupling a double quantum dot capacitively to the second flexural mode of a suspended carbon nanotube, and appropriately tuning the hopping amplitude between the two charge states of the quantum dot, one can introduce a strong anharmonicity in the spectrum of the mechanical mode. This enables one to address directly the first two energy quasi-mechanical eigenstates without populating the third state (cfr. Fig. 4). These two states form a qubit with mainly a mechanical character. Manipulation and read-out is then possible with standard techniques, but at the same time, we found that the coupling to the environment is strongly reduced. The main benefit is the reduction by up to 3-4 orders of magnitude of the pure-dephasing rate, with respect to the double quantum dot. Combined with the expectation of improved dephasing times, this suggests the potential for nanomechanical qubits with very long coherence times. Furthermore, the production of mechanical devices using conventional microfabrication techniques is promising for scalability.

The mechanical qubit can be used to couple to a wide number of modalities for external fields, including acceleration, magnetic forces or other forces. We have shown that any fields that induce forces on the mechanical oscillator can be detected with unprecedented sensitivity, using quantum preparation and detection protocols.

We also found a unitary transformation, valid in the dispersive limit of $g/|t/\hbar - \omega_m| \ll 1$, that maps the problem to the anharmonic oscillator, giving the explicit expressions of the main physical operators in the qubit subspace.

ACKNOWLEDGEMENTS

F.P. acknowledges support from the French *Agence Nationale de la Recherche* (grant SINPHOCOM ANR-19-CE47-0012) and *IDEX Bordeaux* (grant Maesim Risky project 2019 of the LAPHIA Program). A.N.C. acknowledges support from the Army Research Laboratory, the DOE, Office of Basic Energy Sciences, and from the UChicago MRSEC (NSF DMR-1420709). A.B. acknowledges ERC advanced grant number 692876, AGAUR (grant number 2017SGR1664), MICINN grant number RTI2018-097953-B-I00, the Fondo Europeo de Desarrollo, the Spanish Ministry of Economy and Competitiveness through the ‘‘Severo Ochoa’’ program for Centres of Excellence in R&D (CEX2019-000910-S), Fundacio Privada Cellex, Fundacio Mir-Puig, and Generalitat de Catalunya through the CERCA program.

Appendix A: Electrostatics and derivation of the coupling constants

We give here a derivation of the Hamiltonian. For that we need to calculate the electrostatic energy of the system. The only subtle point is the contribution of the voltage sources, as it is well known for the Coulomb blockade problem [55]. One needs the electrostatic energy as a function of the charges in the system, and not of the voltages; this is particularly important for the expression of the mechanical force. Following Ref. 34 (appendix A) the electrostatic problem of N conductors plus a ground conductor can be treated by introducing a capacitance matrix $C_{ij}^{(0)}$ for which the charges on the conductor i can be related to the potentials of the other conductors:

$$Q_i = \sum_{j=0}^N C_{ij}^{(0)} V_j. \quad (A1)$$

Here $C_{ii}^{(0)} = \sum_{i \neq j} c_{ij}$ and $C_{ij}^{(0)} = -c_{ij}$, where c_{ij} is the capacitance between conductor i and j and clearly ${}^t C = C$. We include in the list of conductors the ground with the index 0. The relation given by Eq. (A1) cannot be inverted, since the capacitance matrix has vanishing determinant. This just indicates that one can shift all the potential by a constant. One can then set one of the potential to 0, say the ground, and eliminate one line of the matrix, which we choose to be that related to the charge on the ground. The $N \times N$ capacitance matrix obtained in this way, C_{ij} , is then invertible and one can write

$$V_i = \sum_{j=1}^N (C^{-1})_{ij} Q_j. \quad (A2)$$

The total energy of the system is $U = \sum_{i=0}^N V_i Q_i / 2$. With our choice of $V_0 = 0$, it reduces to $U =$

$\sum_{i=1}^N V_i Q_i / 2 = {}^t V Q / 2$, where we introduced the vector notation for the charge and the potentials. Using the capacitance matrix we have

$$U = \frac{1}{2} {}^t V C V = \frac{1}{2} {}^t Q C^{-1} Q. \quad (\text{A3})$$

In typical problems one needs to include potential sources. These can be modeled with metallic leads with a macroscopic capacitance to the ground $C_B \rightarrow \infty$, and the charge on this island $Q_B \rightarrow \infty$ with $Q_B / C_B = V_B$ constant. In the following, without loss of generality, we will assume that the capacitances of all sources have the same value C_B .

The relevant energy for the problem at hand is the energy expressed as a function of the charges in all the metallic islands and leads. The mechanical displacement x of any mechanical element of the circuit induces a change in the capacitance matrix, which acquires a dependence on the displacement $C(x)$. (For simplicity we consider a single mechanical mode whose displacement is parametrized by the variable x ; generalization to several modes is straightforward.)

The expression for the potential energy is thus

$$U(Q, x) = \frac{1}{2} {}^t Q C(x)^{-1} Q. \quad (\text{A4})$$

From this expression we can find the expression of the potential energy as a function of the charges in the dots and x . We can then eliminate the charges in the leads by using their potentials. For this we need to invert the matrix C exploiting the large C_B limit. Following Ref. 34 we first divide the indices in c and v , for charge nodes and voltage sources, respectively. We can write

$$C = \begin{pmatrix} C_{cc} & C_{cv} \\ C_{vc} & C_{vv} \end{pmatrix}. \quad (\text{A5})$$

The inverse of this matrix can be written as follows

$$(C^{-1})_{cc} = C_{cc}^{-1} + C_{cc}^{-1} C_{cv} D C_{vc} C_{cc}^{-1} \quad (\text{A6})$$

$$(C^{-1})_{vc} = -D C_{vc} C_{cc}^{-1} \quad (\text{A7})$$

$$(C^{-1})_{vv} = C_{vv}^{-1} (1 - C_{vc} C_{cc}^{-1} C_{cv} D) \quad (\text{A8})$$

where $D = (C_{vv} - C_{vc} C_{cc}^{-1} C_{cv})^{-1}$. Since we eliminated the ground metal island, the only macroscopic matrix elements left are in the diagonal part of $C_{vv} \sim C_B$ (cfr. Eq. (A17) in the following). We can then simplify greatly the inverse since to leading order in C_B one has $D = 1/C_B$,

$$(C^{-1})_{cc} = C_{cc}^{-1}, \quad (\text{A9})$$

$$(C^{-1})_{vc} = -C_{vc} C_{cc}^{-1} / C_B, \quad (\text{A10})$$

$$(C^{-1})_{vv} = 1/C_B. \quad (\text{A11})$$

This allows to express the energy as follows:

$$U = \frac{1}{2} {}^t Q_c C_{cc}^{-1} Q_c - {}^t Q_c C_{cc}^{-1} C_{cv} Q_v / C_B + \frac{1}{2} {}^t Q_v Q_v / C_B, \quad (\text{A12})$$

but $Q_v / C_B = V_v$ are the sources voltages and the last term is independent of Q_c . We thus have

$$U = \frac{1}{2} {}^t Q_c C_{cc}^{-1} Q_c - {}^t Q_c C_{cc}^{-1} C_{cv} V_v. \quad (\text{A13})$$

1. Couplings

From this expression we can derive the coupling to the mechanical displacement and to the voltage applied to a nearby gate electrode. For this, we include the x dependence of the capacitances and the substitution $V_v = V_v^{\text{DC}} + V_v^{\text{AC}}$, where V_v^{DC} is the static part and V_v^{AC} the oscillating part of the voltage. If a gate electrode is part of an electromagnetic cavity, one can obtain the coupling to the photon creation and destruction operators via the substitution $V_v^{\text{AC}} = V_v^z (b_v + b_v^\dagger)$, where V_v^z is the zero-point motion voltage of the cavity and b_v the destruction operator for the photons.

We now need a description in terms of the charge fields. Let us associate to each charge variation δq_c^i the occupation operator n_i with eigenvalues 0 or 1 so that the operator for the total number of charges can be written as $Q_c = Q_c^0 + \sum_i n_i \delta q_c^i$. The index i can take into account spin or other degrees of freedom and we included a background frozen charge Q_c^0 . By including this expression into (A13), at lowest order in x we obtain

$$U = U_C + x \sum_i n_i \left(\lambda_i^{\text{em}} + \sum_{j \neq i} n_j \lambda_{ij}^{\text{em}} \right) + \sum_i n_i \lambda_{iv}^{\text{ev}} V_v^{\text{AC}} + x \lambda_v^{\text{mv}} V_v^{\text{AC}} \quad (\text{A14})$$

where

$$U_C = \sum_i n_i {}^t \delta q_c^i C_{cc}^{-1} \left(Q_c^0 - C_{cv} V_v^{\text{DC}} + \sum_j \frac{1}{2} \delta q_c^j n_j \right) \quad (\text{A15})$$

is the pure Coulomb part and the other three terms describe the interaction between the three degrees of freedom x , V^{AC} , and n_i , which are associated with the indices m, v, and e, respectively. (We discarded the constant $U_0 = {}^t Q_c^0 C_{cc}^{-1} Q_c^0 / 2 - {}^t Q_c^0 C_{cc}^{-1} C_{cv} V_v^{\text{DC}}$.) Here

$$\lambda_i^{\text{em}} = \partial_x \left[\left({}^t Q_c^0 + \frac{{}^t \delta q_c^i}{2} \right) C_{cc}^{-1} - V_v^{\text{DC}} C_{vc} C_{cc}^{-1} \right] \delta q_c^i \quad (\text{A16})$$

and $\lambda_{ij}^{\text{em}} = {}^t \delta q_c^i \partial_x C_{cc}^{-1} \delta q_c^j / 2$ are the electromechanical couplings, $\lambda_{iv}^{\text{ev}} = -{}^t \delta q_c^i C_{cc}^{-1} C_{cv}$ the voltage-electron coupling, and $\lambda_v^{\text{mv}} = -{}^t Q_c^0 \partial_x (C_{cc}^{-1} C_{cv})$ the mechanical oscillator-voltage coupling.

2. Single- and double-dot cases

We now consider two examples.

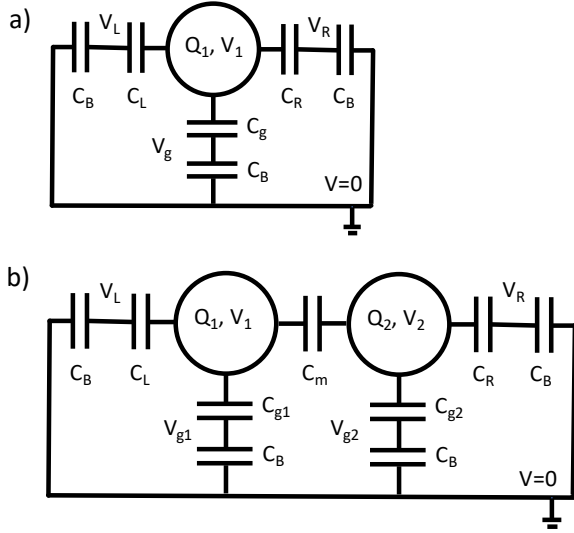


Figure 10. Network of capacitances representing the (a) single- and (b) double-dot circuit. The capacitances C_B are used to model the voltage sources.

(i) The single dot. In this case we have 4 metallic entities, one for the dot, 3 for the left, right and gate leads [cfr. Fig. 10 (a)]. The matrix C reads:

$$C = \begin{pmatrix} C_1 & -C_R & -C_L & -C_g \\ -C_R & C_B + C_R & 0 & 0 \\ -C_L & 0 & C_B + C_L & 0 \\ -C_g & 0 & 0 & C_B + C_g \end{pmatrix} \quad (\text{A17})$$

with obvious notation for the capacitances and with $C_1 = C_L + C_R + C_g$. This gives $C_{cc} = C_1$, $C_{cv} = -(C_R, C_L, C_g)$, and $C_{vv} = C_B + \text{diag}(C_R, C_L, C_g)$. We assume that only C_g depends on x , this gives $\partial_x C_{cc} = \partial_x C_g = C'_g$ and $\partial_x C_{cv} = -C'_g(0, 0, 1)$. We also have $\delta q_c^i = -e$ (with e the electron charge) and for simplicity we report the expressions for $V_L = V_R = 0$. We then have for the couplings

$$\lambda_i^{\text{em}} = eC'_g[Q_0 - (C_1 - C_g)V_g - e/2], \quad (\text{A18})$$

$\lambda_{ij}^{\text{em}} = -e^2 C'_g / (2C_1)$, $\lambda_v^{\text{mv}} = -C'_g Q_0 (C_R, C_L, C_g - C_1) / C_1^2$. The last coupling constant is related to λ^{em} .

(ii) Double dot. Let us consider a double dot, with each dot coupled to a gate voltage [cfr. Fig. 10 (b)]. The capacitance matrix is:

$$C_{cc} = \begin{pmatrix} C_1 & -C_m \\ -C_m & C_2 \end{pmatrix}, \quad (\text{A19})$$

$$C_{cv} = - \begin{pmatrix} C_L & C_{g1} & 0 & 0 \\ 0 & 0 & C_{g2} & C_R \end{pmatrix}, \quad (\text{A20})$$

and $C_{vv} = C_B + \text{diag}(C_L, C_{g1}, C_{g2}, C_R)$. Here $C_i = C_L + C_m + C_{gi}$. We can distinguish two types of n operators, one for the dot 1 (n_1) and the other for the dot

2 (n_2). We have $\delta q_c^1 = (-e, 0)$ and $\delta q_c^2 = (0, -e)$. For simplicity in the following we assume a symmetric situation $C_L = C_R = C$, $V_L = V_R = 0$, $C_1 = C_2 = C_S$, $Q_c^0 = (Q_0, Q_0)$, and $V_v = (0, V_{g1}, V_{g2}, 0)$. For our specific problem, for which the interesting mechanical mode is the second one, we assume that $C_{g1}(x) = C_{g2}(-x)$ by symmetry, so that $C'_{g1} = -C'_{g2}$. With this hypothesis we find for the coupling constants:

$$\begin{aligned} \lambda_1^{\text{em}} + \lambda_2^{\text{em}} &= \frac{eC'_g(C + 2C_m)(e - 4Q_0)(V_{g1} - V_{g2})}{2(C_S^2 - C_m^2)} \\ \lambda_1^{\text{em}} - \lambda_2^{\text{em}} &= \frac{C'_g e [4Q_0 - 2e + eC(V_{g1} + V_{g2})]}{2(C_S^2 - C_m^2)} \\ \lambda_{1v}^{\text{ev}} &= -e \frac{(CC_S, C_g C_S, C_g C_m, CC_m)}{C_S^2 - C_m^2} \\ \lambda_{2v}^{\text{ev}} &= -e \frac{(CC_m, C_g C_m, C_g C_S, CC_S)}{C_S^2 - C_m^2} \\ \lambda_v^{\text{mv}} &= Q_0 C'_g \frac{(-C, 2C_m + C, -2C_m - C, C)}{C_S^2 - C_m^2} \end{aligned}$$

and $\lambda_{12}^{\text{em}} = 0$. For $V_{g1} = V_{g2}$, $\lambda_1^{\text{em}} = -\lambda_2^{\text{em}} = \lambda^{\text{em}}$ leading to the Hamiltonian term that we used in the main text: $\lambda x(n_1 - n_2)$. When we reduce the Hilbert space to the two charge states $(1, 0)$ and $(0, 1)$, this Hamiltonian term can be written as $\lambda x \sigma_z \equiv -\hbar g(x/x_z) \sigma_z$. In this basis $n_1 = (\sigma_z + 1)/2$ and $n_2 = (1 - \sigma_z)/2$. We also have the coupling of the charge of the dots to the voltages of the gate electrodes:

$$H^{\text{ev}} = \frac{eC_g}{2} \left[\mathbf{1} \frac{V_{g1}^{\text{AC}} + V_{g2}^{\text{AC}}}{C_S - C_m} - \sigma_z \frac{V_{g1}^{\text{AC}} - V_{g2}^{\text{AC}}}{C_S + C_m} \right]. \quad (\text{A21})$$

Finally the direct coupling between the mechanical oscillator and the voltages of the gate electrodes is:

$$H^{\text{mv}} = Q_0 C'_g \frac{C + 2C_m}{C_S^2 - C_m^2} x (V_{g1}^{\text{AC}} - V_{g2}^{\text{AC}}). \quad (\text{A22})$$

In order to compare the last two coupling constants we can write this part of the Hamiltonian as follows

$$H = [\lambda^{\text{ev}} \sigma_z / e + \lambda^{\text{mv}} x_z (a + a^\dagger)] V_{g12}^{\text{AC}} \quad (\text{A23})$$

with $\lambda^{\text{ev}} = eC_g(C_S + C_m)/2$, $\lambda^{\text{mv}} = Q_0 C'_g (C + 2C_m) / (C_S^2 - C_m^2)$, $V_{g12}^{\text{AC}} = V_{g1}^{\text{AC}} - V_{g2}^{\text{AC}}$, and we used $x = x_z(a + a^\dagger)$. The ratio of the two coupling constant is then of the order of

$$\frac{\lambda^{\text{mv}} x_z}{\lambda^{\text{ev}} / e} = \frac{Q_0 C'_g}{e C_g} x_z \frac{C + 2C_m}{C_S - C_m} \quad (\text{A24})$$

In general this ratio is small $\sim (Q_0/e)(x_z/L)$ where $L = C_g/C'_g$ is typically of the order of the distance of the nanotube from the gate. Thus the oscillating voltage field couples mainly to the charge degree of freedom.

Appendix B: Mapping of the Hamiltonian on the anharmonic oscillator in the dispersive regime

In this Appendix we show that the Hamiltonian for the system we are considering given by Eq. (1) can be mapped in the dispersive regime on the Hamiltonian of an anharmonic oscillator. We begin by considering H for $\epsilon = 0$. It reduces to $H = t\sigma_x/2 + \hbar\omega_m a^\dagger a - \hbar g(a + a^\dagger)\sigma_z$. Performing a rotation of $\pi/2$ around the y -axis in the charge space with the operator $U_r = e^{-i\pi\sigma_y/4} = (1 - i\sigma_y)/\sqrt{2}$, one has that $U_r^\dagger\sigma_x U_r = \sigma_z$ and $U_r^\dagger\sigma_z U_r = -\sigma_z$, with σ_y left unchanged. The Hamiltonian is then in the standard form for the Rabi model:

$$H_1 = U_r^\dagger H U_r = \frac{t}{2}\sigma_z + \hbar\omega_m a^\dagger a + \hbar g(a + a^\dagger)\sigma_x. \quad (\text{B1})$$

This model has a long history describing the coupling of electromagnetic radiation to a two-level system, but only very recently it has been diagonalized analytically [56]. In practice it is difficult to make use of this solution, but for the case considered in the present paper, an approximate solution, which holds in the so called dispersive limit of $|t - \hbar\omega_m| \ll g$, could be sufficient to obtain an accurate description of the system. As described in Ref. 57, it exists a unitary transformation D_1 such that

$$H_2 = D_1^\dagger H_1 D_1 = t\frac{\sigma_z}{2} + \frac{\hbar\omega_m}{4}(\hat{p}^2 + \hat{x}^2) + \sigma_z \hat{x}^2 \frac{t\hbar g^2}{\Delta^2} + \dots \quad (\text{B2})$$

where we recall $\Delta^2 = t^2 - (\hbar\omega_m)^2$, $\hat{x} = a^\dagger + a$, and $\hat{p} = i(a^\dagger - a)$, with $[\hat{x}, \hat{p}] = 2i$. The Hamiltonian is quadratic in \hat{x} and \hat{p} and commutes with σ_z . It can thus be diagonalized

$$H_2 = t\sigma_z/2 + \sum_{\sigma=\pm} [\omega_\sigma \pi_\sigma (1/2 + c_\sigma^\dagger c_\sigma)], \quad (\text{B3})$$

where

$$\hat{x} = \sum_{\sigma} (\omega_m/\omega_\sigma)^{1/2} (c_\sigma^\dagger + c_\sigma) \pi_\sigma, \quad (\text{B4})$$

$$\hat{p} = \sum_{\sigma} (\omega_\sigma/\omega_m)^{1/2} i(c_\sigma^\dagger - c_\sigma) \pi_\sigma, \quad (\text{B5})$$

and

$$\omega_\sigma = \omega_m [1 + 4\sigma t\hbar g^2/\omega_m \Delta^2]^{1/2} \quad (\text{B6})$$

is the mechanical frequency of each branch, $\pi_\sigma = (1 + \sigma\sigma_z)/2$ is the projector on the σ branch, and $[c_\sigma, c_{\sigma'}^\dagger] = \delta_{\sigma,\sigma'}$. Note that this result reduces to the Born-Oppenheimer picture for $\hbar\omega_m/t \rightarrow 0$. It describes two harmonic oscillators, with different resonating frequencies, the lower branch being softened and the upper being hardened by the interaction.

The transformation found in Ref. [57] allows to simplify the Hamiltonian only at order 2 in $\hbar g/|t - \hbar\omega_m|$. For our purposes we need a transformation allowing to obtain the form of the Hamiltonian up to the quartic terms in \hat{x} . For

this reason we look for an higher-order unitary transformation D that allows to map H_1 to $H_T = D^\dagger H_1 D$ (the full unitary transformation acting on H includes the rotation $U = U_r D$) with H_T given by Eq. (5) of the main text valid at order four in $g/(t/\hbar - \omega_m)$.

In general one can express any unitary transformation as $D = e^A$, where $A = -A^\dagger$. We begin by expressing the transformation of Ref. [57] in terms of the operators \hat{x} and \hat{p} :

$$A_1 = \frac{i\hbar g}{\Delta^2} (t\sigma_y x + \hbar\omega_m \sigma_x p). \quad (\text{B7})$$

The transformed operators can be found using the standard relation:

$$e^A O e^{-A} = \sum_n \frac{1}{n!} C_n^O, \quad (\text{B8})$$

with $C_n^O = [A, C_{n-1}^O]$, and $C_0^O = O$. Performing the expansion at order 2 for $O = H_1$ and $A = A_1$ one obtains the expression for H_2 . Performing the expansion at order 4 generates the sought terms x^4 , but also other terms proportional to $x^3\sigma_x$, $xpx\sigma_y$ and $x^2p^2\sigma_z$. In order to eliminate these terms we add two terms to the A_1 operator so that $A = A_1 + g^3 A_3 + g^4 A_4$. By inspection of the terms generated one can realize that A_3 should involve only cubic terms in \hat{x} and \hat{p} , while A_4 only quartic terms. These terms are multiplied by any of the three Pauli matrices and the unit matrix. This leaves 12 free parameters for A_3 and 15 free parameters for A_4 . By imposing that the cubic and quartic terms (apart from x^4) vanish, we find an explicit expression for A_3 and A_4

$$A_3 = \frac{4it\hbar^3}{3\Delta_3^2\Delta^6} [4\sigma_x t\hbar\omega_m [\hat{x}\hat{p}\hat{x}(3\hbar^2\omega_m^2 - t^2) + 2\hbar^2\omega_m^2\hat{p}^3] + \sigma_y [8t^2\hbar^2\omega_m^2\hat{p}\hat{x}\hat{p} + \hat{x}^3(-t^4 + 6t^2\hbar^2\omega_m^2 + 3\hbar^4\omega_m^4)]] \quad (\text{B9})$$

$$A_4 = \frac{i\sigma_z(\hat{x}^3\hat{p} + \hat{p}\hat{x}^3)t\hbar^5\omega_m(11t^2 - 3\hbar^2\omega_m^2)}{6\Delta_3^2\Delta^6}. \quad (\text{B10})$$

This leads to the Hamiltonian (5) with the coefficients given by Eqs. (6)-(7). Note that the coefficients α_1 and α_2 are very close to one in the limit $\hbar\omega_m/t \ll 1$ since the correction scale like $(\hbar g/t)^4$ and $\hbar^4 g^4 \omega_m^2/t^6$.

We thus have shown that the Born-Oppenheimer picture gives a qualitatively correct description of the problem, even deep in the quantum regime when $\hbar\omega_m$ is not negligible in front of t . This implies a non-trivial unitary transformation that, in contrast with the Born-Oppenheimer picture, mixes the mechanical and charge degrees of freedom. The second important difference is that the coefficients for the quadratic and quartic terms differs from the ones of the semiclassical case. These are of course important if a quantitative description of the anharmonicity is needed.

1. Form of the operators in the qubit Hilbert space

In order to study the decoherence and the way in which the mechanical qubit can be manipulated it is important to obtain the projection of the main operators on the Hilbert subspace formed by the lowest two Hamiltonian eigenstates. This of course can be done numerically in a straightforward way, but it is also useful to have sim-

ple, though approximate, expressions for the form of the operators. For this purpose one can apply the unitary transformations $U = U_r D$, introduced above, to find the expression of the relevant operators in the base for which the Hamiltonian reduces to the form (5) at order g^4 . We are interested by the Pauli matrices for the charge sector and the \hat{x} and \hat{p} operators, for the oscillator sector. Let's define $O^T = U^\dagger O U$.

We obtain:

$$\sigma_x^T = \sigma_z + 2\hbar g \frac{\hat{p}\sigma_y \hbar\omega_m - \sigma_x \hat{x}t}{\Delta^2} - 2\hbar^2 g^2 \frac{\sigma_z \hat{x}^2 t^2 + 2t\hbar\omega_m + \hat{p}^2 \sigma_z (\hbar\omega_m)^2}{\Delta^4} + o(g^3), \quad (\text{B11})$$

$$\sigma_y^T = \sigma_y - 2\hbar^2 g \omega_m \frac{\hat{p}\sigma_x}{\Delta^2} + \hbar^3 g^2 \omega_m \frac{\sigma_x t (\hat{x}\hat{p} + \hat{p}\hat{x}) - 2\hat{p}^2 \sigma_y \hbar\omega_m}{\Delta^4} + o(g^3), \quad (\text{B12})$$

$$\sigma_z^T = -\sigma_x - 2\hbar g t \frac{\hat{x}\sigma_z}{\Delta^2} + \hbar^2 g^2 t \frac{2\sigma_z \hat{x}^2 t - \sigma_y \hbar\omega_m (\hat{x}\hat{p} + \hat{p}\hat{x})}{\Delta^4} + o(g^3), \quad (\text{B13})$$

$$\hat{x}^T = \hat{x} + 2\hbar^2 g \omega_m \frac{\sigma_x}{\Delta^2} + 2\hbar^3 g^2 \frac{\sigma_z \hat{x} t \omega_m}{\Delta^4} + o(g^3), \quad (\text{B14})$$

$$\hat{p}^T = \hat{p} - 2\hbar g t \frac{\sigma_y}{\Delta^2} + 2\hbar^3 g^2 \frac{\sigma_z \hat{p} t \omega_m}{\Delta^4} + o(g^3). \quad (\text{B15})$$

The projection in the subspace of the first two-excited states can be readily calculated by neglecting the quartic term of the Hamiltonian given by Eq. (5). This implies a scaling of the \hat{x} and \hat{p} operators by the factor ξ defined by Eq. (9): $\hat{x} \rightarrow \xi \hat{x}$ and $\hat{p} \rightarrow \hat{p}/\xi$. The result at order 4 in g gives that only 6 components are non-vanishing, out of the possible 16. These are given by Eq. (11) and Eq. (12) in the main text. The expression for the β coefficient is

given in the main text (13)-(18) to order g^2 . From these expression one can see how the different degrees of freedom are mixed by the interaction. For instance, the displacement acquires a σ_x component, which in this basis is the charge operator. On the other side the charge operator σ_z acquires a component of the displacement operator. We give here the g^3 and g^4 terms (we use $\hbar = 1$ in these expressions):

$$\beta_{14} = \frac{16t (6\omega_m^2 t^3 (9\xi^4 + 2) \xi^4 - 4\omega_m^3 t^2 (15\xi^4 + 16) \xi^2 + 9\omega_m^4 t (3\xi^8 + 4\xi^4 + 8) - 18\omega_m^5 \xi^6 + 14\omega_m t^4 \xi^6 - 9t^5 \xi^8)}{3\Delta^8 \Delta_3^2 \xi^4} \quad (\text{B16})$$

$$\beta_{24} = \frac{16t (-4\omega_m^2 t^3 (9\xi^4 + 2) \xi^4 + 2\omega_m^3 t^2 (15\xi^4 + 16) \xi^2 - 6\omega_m^4 t (3\xi^8 + 4\xi^4 + 8) + 9\omega_m^5 \xi^6 - 7\omega_m t^4 \xi^6 + 6t^5 \xi^8)}{3\Delta^8 \Delta_3^2 \xi^4} \quad (\text{B17})$$

$$\beta_{33} = \frac{96\omega_m^3 t^2 (\xi^4 + 2) - 32\omega_m t^4 \xi^4}{3\Delta^6 \Delta_3^2 \xi^3} \quad (\text{B18})$$

$$\beta_{43} = \frac{8 (2\omega_m^2 t^3 (9\xi^4 + 4) + 9\omega_m^4 t \xi^4 - 3t^5 \xi^4)}{3\Delta^6 \Delta_3^2 \xi} \quad (\text{B19})$$

$$\beta_{54} = \frac{2\omega_m t (3\xi^4 (-58\omega_m^2 t^2 - 15\omega_m^4 + 9t^4) - 64\omega_m^2 t^2 - 96\omega_m t \xi^2 (t - \omega_m)(\omega_m + t))}{3\Delta^8 \Delta_3^2 \xi} \quad (\text{B20})$$

$$\beta_{64} = \frac{2\omega_m t (\xi^4 (-66\omega_m^2 t^2 - 27\omega_m^4 + 29t^4) - 192\omega_m^2 t^2 + 96\omega_m t \xi^2 (t - \omega_m)(\omega_m + t))}{3\Delta^8 \Delta_3^2 \xi^3}. \quad (\text{B21})$$

[1] S. Barzanjeh, D. Vitali, P. Tombesi, and G. J. Milburn, Entangling optical and microwave cavity modes by means

of a nanomechanical resonator, Phys. Rev. A **84**, 042342

- (2011).
- [2] T. A. Palomaki, J. W. Harlow, J. D. Teufel, R. W. Simmonds, and K. W. Lehnert, Coherent state transfer between itinerant microwave fields and a mechanical oscillator, *Nature* **495**, 210 (2013).
 - [3] R. W. Andrews, R. W. Peterson, T. P. Purdy, K. Cicak, R. W. Simmonds, C. A. Regal, and K. W. Lehnert, Bidirectional and efficient conversion between microwave and optical light, *Nat. Phys.* **10**, 321 (2014).
 - [4] F. Lecocq, J. B. Clark, R. W. Simmonds, J. Aumentado, and J. D. Teufel, Mechanically Mediated Microwave Frequency Conversion in the Quantum Regime, *Phys. Rev. Lett.* **116**, 043601 (2016).
 - [5] A. Vainsencher, K. J. Satzinger, G. A. Peairs, and A. N. Cleland, Bi-directional conversion between microwave and optical frequencies in a piezoelectric optomechanical device, *Appl. Phys. Lett.* **109**, 033107 (2016).
 - [6] J. Bochmann, A. Vainsencher, D. D. Awschalom, and A. N. Cleland, Nanomechanical coupling between microwave and optical photons, *Nat. Phys.* **9**, 712 (2013).
 - [7] C. F. Ockeloen-Korppi, E. Damskäg, J.-M. Pirkkalainen, A. A. Clerk, M. J. Woolley, and M. A. Sillanpää, Quantum Backaction Evading Measurement of Collective Mechanical Modes, *Phys. Rev. Lett.* **117**, 140401 (2016).
 - [8] P. Rabl, S. J. Kolkowitz, F. H. L. Koppens, J. G. E. Harris, P. Zoller, and M. D. Lukin, A quantum spin transducer based on nanoelectromechanical resonator arrays, *Nat. Phys.* **6**, 602 (2010).
 - [9] K. Stannigel, P. Rabl, A. S. Sørensen, P. Zoller, and M. D. Lukin, Optomechanical Transducers for Long-Distance Quantum Communication, *Phys. Rev. Lett.* **105**, 220501 (2010).
 - [10] K. J. Satzinger, Y. P. Zhong, H.-S. Chang, G. A. Peairs, A. Bienfait, M.-H. Chou, A. Y. Cleland, C. R. Conner, É. Dumur, J. Grebel, I. Gutierrez, B. H. November, R. G. Povey, S. J. Whiteley, D. D. Awschalom, D. I. Schuster, and A. N. Cleland, Quantum control of surface acoustic-wave phonons, *Nature* **563**, 661 (2018).
 - [11] A. Bienfait, K. J. Satzinger, Y. P. Zhong, H.-S. Chang, M.-H. Chou, C. R. Conner, É. Dumur, J. Grebel, G. A. Peairs, R. G. Povey, and A. N. Cleland, Phonon-mediated quantum state transfer and remote qubit entanglement, *Science* **364**, 368 (2019).
 - [12] A. Bienfait, Y. P. Zhong, H.-S. Chang, M.-H. Chou, C. R. Conner, É. Dumur, J. Grebel, G. A. Peairs, R. G. Povey, K. J. Satzinger, and A. N. Cleland, Quantum Erasure Using Entangled Surface Acoustic Phonons, *Phys. Rev. X* **10**, 021055 (2020).
 - [13] C. L. Degen, F. Reinhard, and P. Cappellaro, Quantum sensing, *Rev. Mod. Phys.* **89**, 10.1103/RevModPhys.89.035002 (2017).
 - [14] C. Urgell, W. Yang, S. L. De Bonis, C. Samanta, M. J. Esplandiú, Q. Dong, Y. Jin, and A. Bachtold, Cooling and self-oscillation in a nanotube electromechanical resonator, *Nat. Phys.* **16**, 32 (2020).
 - [15] G. S. MacCabe, H. Ren, J. Luo, J. D. Cohen, H. Zhou, A. Sipahigil, M. Mirhosseini, and O. Painter, Nanoacoustic resonator with ultralong phonon lifetime, *Science* **370**, 840 (2020).
 - [16] F. Arute, K. Arya, R. Babbush, D. Bacon, J. C. Bardin, R. Barends, R. Biswas, S. Boixo, F. G. S. L. Brandao, D. A. Buell, B. Burkett, Y. Chen, Z. Chen, B. Chiaro, R. Collins, W. Courtney, A. Dunsworth, E. Farhi, B. Foxen, A. Fowler, C. Gidney, M. Giustina, R. Graff, K. Guerin, S. Habegger, M. P. Harrigan, M. J. Hartmann, A. Ho, M. Hoffmann, T. Huang, T. S. Humble, S. V. Isakov, E. Jeffrey, Z. Jiang, D. Kafri, K. Kechedzhi, J. Kelly, P. V. Klimov, S. Knysh, A. Korotkov, F. Kostritsa, D. Landhuis, M. Lindmark, E. Lucero, D. Lyakh, S. Mandrà, J. R. McClean, M. McEwen, A. Megrant, X. Mi, K. Michielsen, M. Mohseni, J. Mutus, O. Naaman, M. Neeley, C. Neill, M. Y. Niu, E. Ostby, A. Petukhov, J. C. Platt, C. Quintana, E. G. Rieffel, P. Roushan, N. C. Rubin, D. Sank, K. J. Satzinger, V. Smelyanskiy, K. J. Sung, M. D. Trevithick, A. Vainsencher, B. Villalonga, T. White, Z. J. Yao, P. Yeh, A. Zalcman, H. Neven, and J. M. Martinis, Quantum supremacy using a programmable superconducting processor, *Nature* **574**, 505 (2019).
 - [17] C. Rigetti, J. M. Gambetta, S. Poletto, B. L. T. Plourde, J. M. Chow, A. D. Córcoles, J. A. Smolin, S. T. Merkel, J. R. Rozen, G. A. Keefe, M. B. Rothwell, M. B. Ketchen, and M. Steffen, Superconducting qubit in a waveguide cavity with a coherence time approaching 0.1 ms, *Phys. Rev. B* **86**, 100506 (2012).
 - [18] S. Rips and M. J. Hartmann, Quantum Information Processing with Nanomechanical Qubits, *Phys. Rev. Lett.* **110**, 120503 (2013).
 - [19] S. Rips, I. Wilson-Rae, and M. J. Hartmann, Nonlinear nanomechanical resonators for quantum optoelectromechanics, *Phys. Rev. A* **89**, 013854 (2014).
 - [20] A. D. Armour, M. P. Blencowe, and Y. Zhang, Classical dynamics of a nanomechanical resonator coupled to a single-electron transistor, *Phys. Rev. B* **69**, 125313 (2004).
 - [21] Y. M. Blanter, O. Usmani, and a. Y. V. Nazarov, Single-Electron Tunneling with Strong Mechanical Feedback, *Phys. Rev. B* **93**, 136802 (2004).
 - [22] N. M. Chtchelkatchev, W. Belzig, and C. Bruder, Charge transport through a single-electron transistor with a mechanically oscillating island, *Phys. Rev. B* **70**, 193305 (2004).
 - [23] A. A. Clerk and S. Bennett, Quantum nanoelectromechanics with electrons, quasi-particles and Cooper pairs: Effective bath descriptions and strong feedback effects, *New J. of Phys.* **7**, 238 (2005).
 - [24] J. Koch and F. von Oppen, Franck-Condon Blockade and Giant Fano Factors in Transport through Single Molecules, *Phys. Rev. Lett.* **94**, 206804 (2005).
 - [25] D. Mozyrsky, M. B. Hastings, and I. Martin, Intermittent polaron dynamics: Born-Oppenheimer approximation out of equilibrium, *Phys. Rev. B* **73**, 035104 (2006).
 - [26] C. B. Doiron, W. Belzig, and C. Bruder, Electrical transport through a single-electron transistor strongly coupled to an oscillator, *Phys. Rev. B* **74**, 205336 (2006).
 - [27] F. Pistolesi and S. Labarthe, Current blockade in classical single-electron nanomechanical resonator, *Phys. Rev. B* **76**, 165317 (2007).
 - [28] S. L. de Bonis, C. Urgell, W. Yang, C. Samanta, A. Noury, J. Vergara-Cruz, Q. Dong, Y. Jin, and A. Bachtold, Ultrasensitive Displacement Noise Measurement of Carbon Nanotube Mechanical Resonators, *Nano Lett.* **18**, 5324 (2018).
 - [29] I. Khivrich, A. A. Clerk, and S. Ilani, Nanomechanical pump-probe measurements of insulating electronic states in a carbon nanotube, *Nat. Nanotechnol.* **14**, 161 (2019).

- [30] S. Blien, P. Steger, N. Hüttner, R. Graaf, and A. K. Hüttel, Quantum capacitance mediated carbon nanotube optomechanics, *Nat. Comm.* **11**, 1636 (2020).
- [31] Y. Wen, N. Ares, F. J. Schupp, T. Pei, G. a. D. Briggs, and E. A. Laird, A coherent nanomechanical oscillator driven by single-electron tunnelling, *Nat. Phys.* **16**, 75 (2020).
- [32] A. Benyamini, A. Hamo, S. V. Kusminskiy, F. von Oppen, and S. Ilani, Real-space tailoring of the electron–phonon coupling in ultraclean nanotube mechanical resonators, *Nat. Phys.* **10**, 151 (2014).
- [33] A. Hamo, A. Benyamini, I. Shapir, I. Khivrich, J. Waissman, K. Kaasbjerg, Y. Oreg, F. von Oppen, and S. Ilani, Electron attraction mediated by Coulomb repulsion, *Nature* **535**, 395 (2016).
- [34] W. G. van der Wiel, S. De Franceschi, J. M. Elzerman, T. Fujisawa, S. Tarucha, and L. P. Kouwenhoven, Electron transport through double quantum dots, *Rev. Mod. Phys.* **75**, 1 (2002).
- [35] M. Galperin, M. A. Ratner, and A. Nitzan, Hysteresis, Switching, and Negative Differential Resistance in Molecular Junctions: A Polaron Model, *Nano Lett.* **5**, 125 (2005).
- [36] G. Micchi, R. Avriller, and F. Pistolesi, Mechanical Signatures of the Current Blockade Instability in Suspended Carbon Nanotubes, *Phys. Rev. Lett.* **115**, 206802 (2015).
- [37] R. Avriller, B. Murr, and F. Pistolesi, Bistability and displacement fluctuations in a quantum nanomechanical oscillator, *Phys. Rev. B* **97**, 155414 (2018).
- [38] F. T. Hioe and E. W. Montroll, Quantum theory of anharmonic oscillators. I. Energy levels of oscillators with positive quartic anharmonicity, *J. Math. Phys.* **16**, 1945 (1975).
- [39] J. A. Schreier, A. A. Houck, J. Koch, D. I. Schuster, B. R. Johnson, J. M. Chow, J. M. Gambetta, J. Majer, L. Frunzio, M. H. Devoret, S. M. Girvin, and R. J. Schoelkopf, Suppressing charge noise decoherence in superconducting charge qubits, *Phys. Rev. B* **77**, 180502 (2008).
- [40] F. T. Hioe, D. MacMillen, and E. W. Montroll, Quantum theory of anharmonic oscillators: Energy levels of a single and a pair of coupled oscillators with quartic coupling, *Phys. Rep.* **43**, 305 (1978).
- [41] E. Collin, G. Ithier, A. Aassime, P. Joyez, D. Vion, and D. Esteve, NMR-like Control of a Quantum Bit Superconducting Circuit, *Phys. Rev. Lett.* **93**, 157005 (2004).
- [42] J. Majer, J. M. Chow, J. M. Gambetta, J. Koch, B. R. Johnson, J. A. Schreier, L. Frunzio, D. I. Schuster, A. A. Houck, A. Wallraff, A. Blais, M. H. Devoret, S. M. Girvin, and R. J. Schoelkopf, Coupling superconducting qubits via a cavity bus, *Nature* **449**, 443 (2007).
- [43] A. A. Houck, J. A. Schreier, B. R. Johnson, J. M. Chow, J. Koch, J. M. Gambetta, D. I. Schuster, L. Frunzio, M. H. Devoret, S. M. Girvin, and R. J. Schoelkopf, Controlling the Spontaneous Emission of a Superconducting Transmon Qubit, *Phys. Rev. Lett.* **101**, 080502 (2008).
- [44] A. Blais, R.-S. Huang, A. Wallraff, S. M. Girvin, and R. J. Schoelkopf, Cavity quantum electrodynamics for superconducting electrical circuits: An architecture for quantum computation, *Phys. Rev. A* **69**, 062320 (2004).
- [45] T. Frey, P. J. Leek, M. Beck, A. Blais, T. Ihn, K. Ensslin, and A. Wallraff, Dipole Coupling of a Double Quantum Dot to a Microwave Resonator, *Phys. Rev. Lett.* **108**, 046807 (2012).
- [46] P. Scarlino, D. J. van Woerkom, A. Stockklauser, J. V. Koski, M. C. Collodo, S. Gasparinetti, C. Reichl, W. Wegscheider, T. Ihn, K. Ensslin, and A. Wallraff, All-Microwave Control and Dispersive Readout of Gate-Defined Quantum Dot Qubits in Circuit Quantum Electrodynamics, *Phys. Rev. Lett.* **122**, 206802 (2019).
- [47] J. Hauss, A. Fedorov, S. André, V. Brosco, C. Hutter, R. Kothari, S. Yeshwanth, A. Shnirman, and G. Schön, Dissipation in circuit quantum electrodynamics: Lasing and cooling of a low-frequency oscillator, *New J. Phys.* **10**, 095018 (2008).
- [48] C. Cohen-Tannoudji, J. Dupont-Roc, and G. Grynberg, *Atom-Photon Interactions: Basic Processes and Applications* (Wiley, New York, 1992).
- [49] W. Yang, C. Urgell, S. L. De Bonis, M. Marganska, M. Grifoni, and A. Bachtold, Fabry-Pérot oscillations in correlated carbon nanotubes, arXiv:2003.08226 [cond-mat] (2020), arXiv:2003.08226 [cond-mat].
- [50] J. J. Viennot, M. C. Dartiailh, A. Cottet, and T. Kontos, Coherent coupling of a single spin to microwave cavity photons, *Science* **349**, 408 (2015).
- [51] E. Hebestreit, M. Frimmer, R. Reimann, and L. Novotny, Sensing Static Forces with Free-Falling Nanoparticles, *Phys. Rev. Lett.* **121**, 063602 (2018).
- [52] H. J. Hug, B. Stiefel, P. J. A. van Schendel, A. Moser, S. Martin, and H.-J. Güntherodt, A low temperature ultrahigh vacuum scanning force microscope, *Review of Scientific Instruments* **70**, 3625 (1999).
- [53] M. Ribezzi-Crivellari, J. M. Huguet, and F. Ritort, Counter-propagating dual-trap optical tweezers based on linear momentum conservation, *Review of Scientific Instruments* **84**, 043104 (2013).
- [54] A. A. Clerk, M. H. Devoret, S. M. Girvin, F. Marquardt, and R. J. Schoelkopf, Introduction to quantum noise, measurement, and amplification, *Reviews of Modern Physics* **82**, 1155 (2010).
- [55] H. Grabert and M. H. Devoret, *Single Charge Tunneling: Coulomb Blockade Phenomena In Nanostructures* (Springer Science & Business Media, 2013).
- [56] D. Braak, Integrability of the Rabi Model, *Phys. Rev. Lett.* **107**, 100401 (2011).
- [57] D. Zueco, G. M. Reuther, S. Kohler, and P. Hänggi, Qubit-oscillator dynamics in the dispersive regime: Analytical theory beyond the rotating-wave approximation, *Phys. Rev. A* **80**, 033846 (2009).